

Synthesis and Corrosion Resistance of ZnAl Layered Double Hydroxide Film on Q235 Steel

Shuyu Xie^{1,2}, Jihui Wang^{1,2,*}, Wenbin Hu²

¹ State Key Laboratory of Hydraulic Engineering Simulation and Safety, Tianjin University, Tianjin 300072, P R China

² Tianjin Key Laboratory of Composite and Functional Materials, School of Materials Science and Engineering, Tianjin University, Tianjin 300072, P R China

*E-mail: jhwang@tju.edu.cn

Received: 8 March 2019 / Accepted: 29 April 2019 / Published: 10 June 2019

ZnAl-MoO₄-LDHs film was fabricated in situ on the Q235 steel substrate by aluminizing process, coprecipitation method and ion-exchange method. The morphology, composition and structure of the LDHs film were analyzed by scanning electron microscopy (SEM), X-ray diffraction (XRD) and Fourier transform infrared (FT-IR) spectroscopy. The anticorrosion capability of the Q235 steel with LDHs film was observed by electrochemical impedance spectroscopy (EIS) and polarization curve. The LDHs film had a plate-like morphology which is the typical grain morphology of LDHs, and a particle size ranging from 2 μm to 4 μm and a particle thickness ranging from 0.05 μm to 0.2 μm. The increase of the layer spacing of LDHs film and the absorption peak of MoO₄²⁻ in FT-IR spectra can prove the intercalation of MoO₄²⁻. Compared with bare Q235 steel, the corrosion current density of the Q235 steel with LDHs film decreased and the polarization resistance increased. The improvement of corrosion resistance is owed to the LDHs film which plays as a barrier between the substrate and the corrosive medium. The exchangeability of the interlayered anions of LDHs can catch the corrosive chloride ion in the medium and the MoO₄²⁻ released from the LDHs layer can play as corrosion inhibitor.

Keywords: layered double hydroxide film; corrosion protection; in-situ growth; carbon steel

1. INTRODUCTION

Steel has been the most widely used material in the world since it was put into industrial production. Steel can be corroded easily in natural environment, which has brought great economic loss and waste of resources[1-3]. The demand for steel products with great corrosion resistance is growing rapidly[4]. Surface modification can improve the corrosion resistance of steel and reduce economic losses and security risks [5, 6].

Surface treatment is used to improve the corrosion resistance of metal, including surface coating and preparation of surface conversion layer[7, 8]. The common anti-corrosive treatments of metal include anodic oxidation and chemical oxidation[9, 10]. However, both of the processes require a large number of electrolytes, such as sulfate, chromate and phosphate, which will cause serious environmental concerns. The research and development of non-toxic and harmless anti-corrosion technology is significant[11].

Layered double hydroxides (LDHs), which is known as hydrotalcite-like compounds (HTLc), is a layered anionic material with a general formula of $[M_{1-x}^{2+}M_x^{3+}(\text{OH})_2]^{x+}(A^{n-})_{x/n} \cdot m\text{H}_2\text{O}$. M^{2+} and M^{3+} are the divalent and trivalent metals, and A^{n-} is the intercalated anion[12, 13]. Studies have shown that LDHs can be applied in metal corrosion protection [14, 15]. For examples, LDHs can be mixed with organic paint for metal surface coating, or used to form a dense and strong film on metal substrate by in-situ growth method [16-18]. For the first application, LDHs powder is mixed with organic coating, which can provide corrosion protection by the exchangeability of intercalated anions in LDHs. When the coating is in contact with corrosive medium, the intercalated corrosion-inhibiting ions is released and the corrosive ions is absorbed into LDHs. Coating with LDHs can not only passivate the surface of the metal, but also reduce corrosive ions in the medium surrounding the matrix[19]. Mahajanam[20] has suggested that ZnAl-[V10O28]6- LDHs can provide barrier protection and active protection as a corrosion inhibiting pigment additive for protective organic coatings.

Although mixing LDHs powder into organic coating can effectively improve the corrosion resistance of metal, there are still some problems, such as the weak binding with metal substrate, heterogeneous dispersion of LDHs powder and poor thermostability^[20]. To solve the above problems, immobilization of the LDHs meets the trend of the moment in the field of metal corrosion protection. LDHs film material has stronger binding with the metal substrate and it can be dense and uniform, which is more favorable for metal corrosion resistance [21-23].

Guo et al. crystallized ZnAl-NO₃-LDHs films on the aluminum substrate by hydrothermal method, which exhibited a low corrosion current density value and had a strong adhesion with the substrate[24]. This method not only saves energy, but also simplifies the synthesis process of LDHs film. Further research of this LDHs film shows that it has good corrosion resistance due to the exchangeability of intercalated anions in the film. After immersion test in the corrosive electrolyte, the intercalated anion was Cl⁻, which means there was ion exchange reaction between NO₃⁻ in interlayer of LDHs film and Cl⁻ in the corrosive medium. Concentration of Cl⁻ was reduced, leading to corrosion protection of the aluminum substrate.

For the anti-corrosion of metal materials, the main direction of the current research is to develop environmental friendly materials with good corrosion resistance and non-toxicity. In our work, we firstly treated the Q235 steel with aluminizing technology by pack cementation to get an iron aluminide intermetallic coating. Then we fabricated ZnAl-NO₃-LDHs film on the aluminized steel substrate and treated it with Na₂MoO₄ solution to gain the ZnAl-MoO₄-LDHs film, which can provide good corrosion resistance for the substrate.

2. EXPERIMENTAL

2.1. Materials

Q235 steel (10mm×10mm×3mm pieces). Aluminum powder(200-300 mesh), hydrochloric acid purchased from Titan Technology Co. Ltd. Ammonium chloride, aluminium oxide, ammonium nitrate, sodium hydroxide and sodium molybdate purchased from Aladdin Industrial Corporation. Zinc nitrate, sodium carbonate and ammonium hydroxide purchased from Tianjin Guangfu Fine Chemical Research Institute.

2.2. Aluminizing of Q235 steel

The Q235 steel pieces were abraded using SiC paper up to 1000 grit. Then the samples were rinsed in a mixed alkaline solution (6wt% NaOH, 8wt% Na₂CO₃) and 5wt% solution of hydrochloric acid respectively by ultrasonic cleaning. The samples were put into a heat-resisting stainless steel jar and packed with aluminizing medium (wt% Al: Al₂O₃: NH₄Cl=49:49:2). The jar was put into a muffle furnace, which was heated up to 650°C at a rate of about 10°C per minute and kept the temperature for 4 hours. After that, the jar was cooled inside the furnace to room temperature. The aluminized Q235 pieces were rinsed by ethanol and dried at room temperature.

2.3. Synthesis of ZnAl-NO₃-LDHs film

0.1875g Al(NO₃)₃ and 0.48g NH₄NO₃ was dissolved in 120mL DI water at first. Then 100mL of 10wt% ammonia solution was prepared. The pH of the mixed solution of Al(NO₃)₃ and NH₄NO₃ was adjusted to 10 with 10wt% ammonia solution accurately by using a pH detector. Then the solution was transferred to a reaction kettle made of PTFE and the aluminized Q235 pieces were immersed into the solution. The reaction kettle was kept in the oven at 120°C for 10 hours. After that, the samples were rinsed by ethanol and dried at room temperature. Thus the ZnAl-NO₃-LDHs film grew in-situ on the aluminized Q235 steel. To modify the surface of the LDHs film, samples with ZnAl-NO₃-LDHs film were immersed into a 0.05M Na₂MoO₄ (50mL) solution at 45°C for 3 hours. Finally the samples was rinsed by ethanol and dried at room temperature and the ZnAl-MoO₄-LDHs film was obtained.

2.4. Surface characterization

The surface morphology of the LDHs film samples was observed by using Hatchi S-4800 scanning electron microscopy (SEM) with an accelerating voltage of 15 kV. The elemental composition of the LDHs film were measured by the energy dispersive spectroscopy (EDS, Genesis XM2, EDAX, USA) at 15 kV accelerating voltage. The crystal structure of the LDHs film samples was determined by Rigaku D/MAX 2500X X-ray diffractometer (XRD) at a scan speed of 5°/min in the 2θ range of 5–89° with Cu-K alpha radiation at a wavelength of 0.154 nm. FT-IR spectra of the LDHs film samples were analyzed by using a BIO-RAD 3000 spectrophotometer.

2.5. Electrochemical test

The electrochemical measurements were conducted in a 3.5wt% NaCl solution at room temperature. A three-electrode system was used to measure the corrosion behaviors of the Q235 samples with LDHs film on Autolab 302 electrochemical workstation, including the electrochemical impedance spectroscopy (EIS) test and the polarization curves test. The Q235 samples with LDHs film covering the surface were used as the working electrode (WE) with a working area of 1cm². A platinum plate was used as the counter electrode (CE) and a saturated calomel electrode (SCE) was used as the reference electrode (RE).

The measuring frequency of the EIS test range was from 10⁵ Hz to 10⁻² Hz with an amplitude of 10mV under the open circuit potential (OCP). After that, the EIS spectra were analyzed by ZsimpWin software using appropriate equivalent circuit. The polarization curves of the samples were measured from -0.1V versus OCP (SCE) to 0.1V versus OCP (SCE) at the speed of 0.1V/min. Then the corrosion potential (E_{corr}) and the current density (I_{corr}) of the samples were analyzed and calculated.

The protection efficiency of different LDHs film in 3.5 wt% NaCl solution can be calculated by the following equation:

$$\eta_1 = \frac{I_{\text{corr}} - I'_{\text{corr}}}{I_{\text{corr}}} \times 100\%$$

$$\eta_2 = \frac{R_{\text{total}} - R'_{\text{total}}}{R_{\text{total}}} \times 100\%$$

I'_{corr} is the current density of different samples in 3.5 wt% NaCl, and I_{corr} is the current density of bare Q235 steel in 3.5 wt% NaCl. R_{total} is the polarization resistance of different samples in 3.5 wt% NaCl and R'_{total} is the polarization resistance of bare Q235 steel in 3.5 wt% NaCl.

2.6. Release test

Samples with ZnAl-MoO₄-LDHs film were immersed into the 3.5wt% NaCl solution for 24 hours. After that, the concentration of MoO₄²⁻ was test by Agilent 7700× inductively coupled plasma mass spectrometer (ICP-MS).

3. RESULTS

3.1. Surface characterization

The SEM images and EDS detection results for different samples are shown in Figure 1. The surface morphology of the aluminized Q235 steel is granulated due to the grain growth of Fe₂Al₅. The LDHs film clearly has a plate-like shape and grows vertically on the substrate, whereas the LDHs crystal demonstrates an aggregate growth in some areas of the film. The LDHs have a particle size ranging from 2 μm to 4 μm and a particle thickness ranging from 0.05 μm to 0.2 μm. Wu et al. synthesized LDHs film

on anodized magnesium alloy AZ31 with similar plate-like LDH crystallites and observed a fine and compact film[25].

The EDS results reveal that the surface of the aluminized Q235 steel is mainly composed of Fe element and Al with atomic percentage of 26.78% and 67.64%, respectively. Minimal traces of O can be found on the surface because of the oxidation of the substrate. As the ZnAl-NO₃-LDHs film grows, the atomic percentage of Al decreases to 14.12% while Zn, O, and N with atomic percentages of 20.37%, 64.07%, and 1.44%, respectively, begin to appear. After surface treatment with Na₂MoO₄, Mo with an atomic percentage of 0.56% starts to appear in the EDS detection whereas N completely disappears, thereby indicating the exchange of interlayer anions between MoO₄²⁻ and NO₃⁻.

Figures 2 and 3 present the side-view SEM images and results of the EDS mapping, respectively. Figure 4 shows that the LDHs film has a thickness of approximately 7 μm and has an aluminized layer with a thickness of 10 μm, thereby suggesting that not all aluminized layers have been transferred to LDHs. The appearance of Mo in Figure 5 indicates the exchange of interlayer anions between MoO₄²⁻ and NO₃⁻.

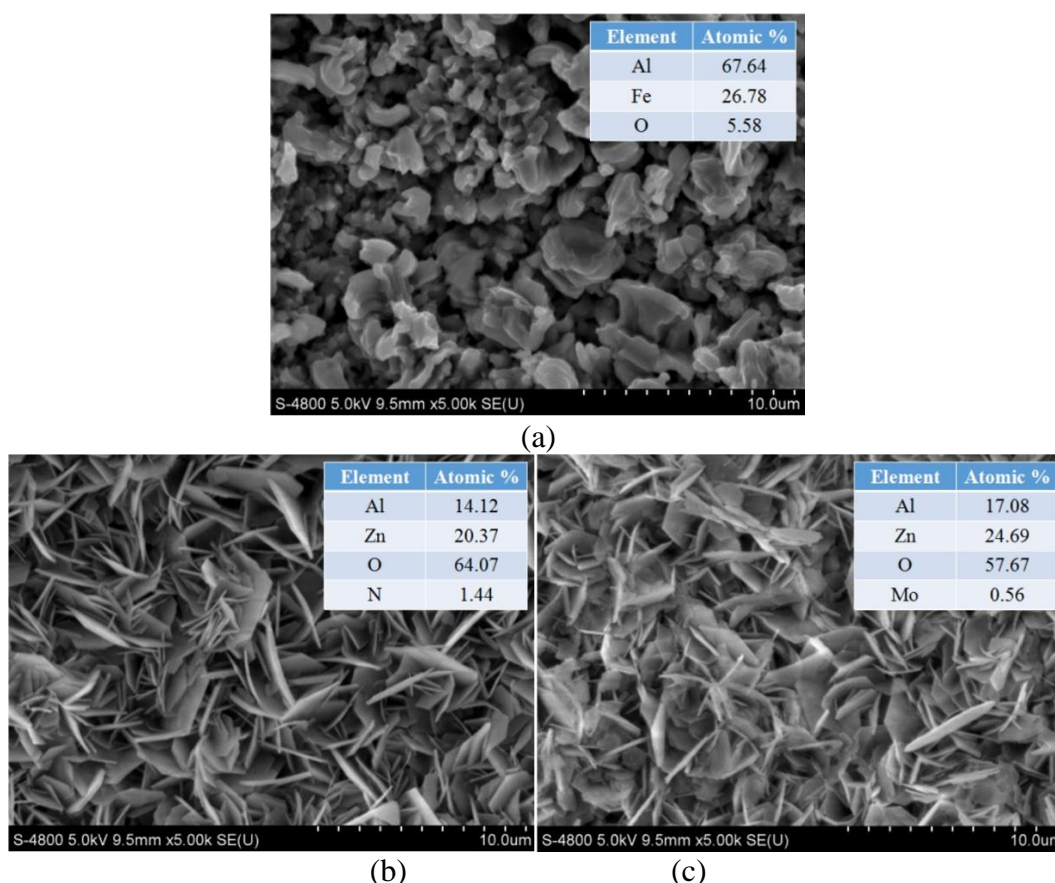


Figure 1. SEM images and EDS detection of (a) Aluminized Q235 steel; (b) ZnAl-NO₃-LDHs film; (c) ZnAl-MoO₄-LDHs film

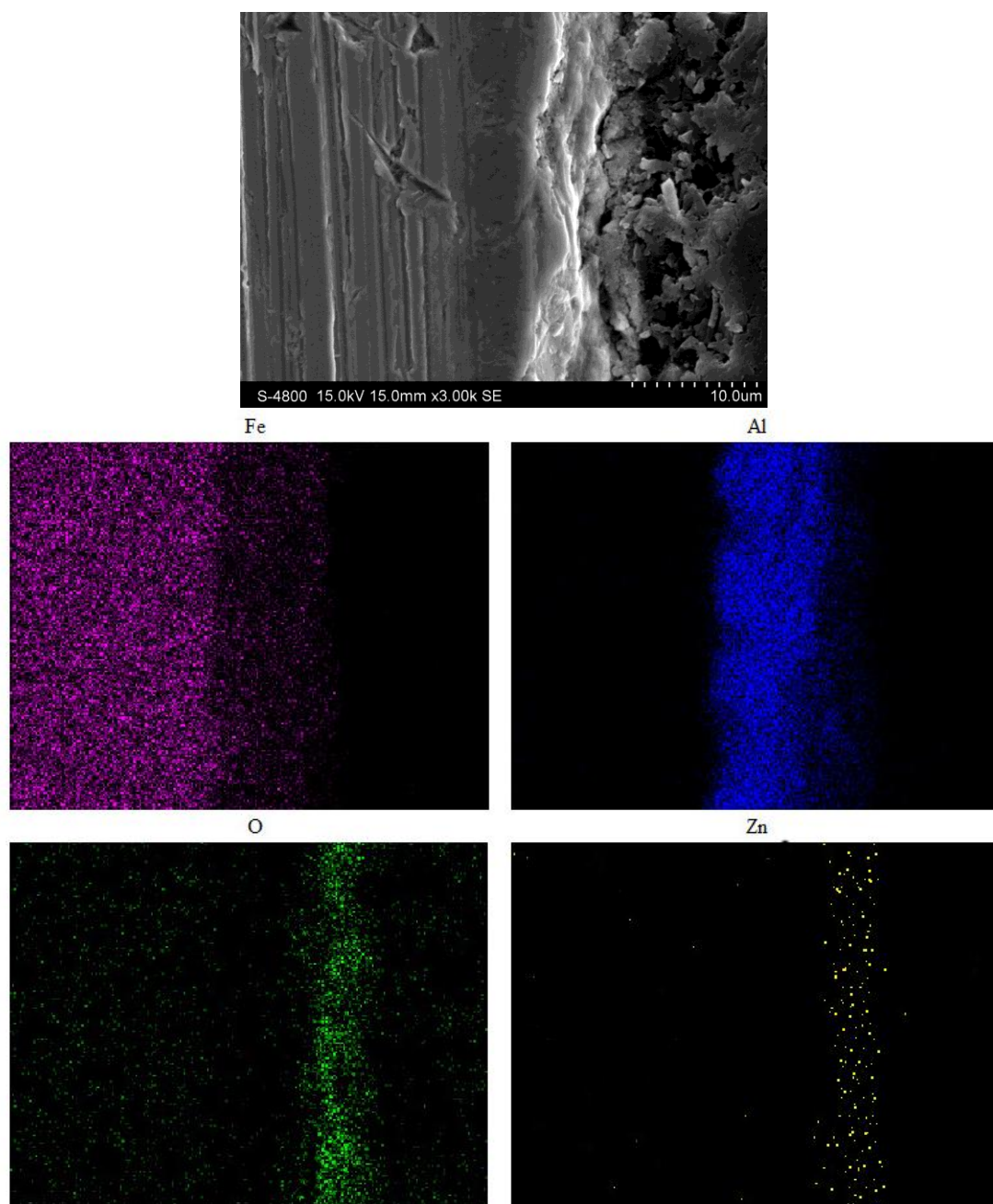
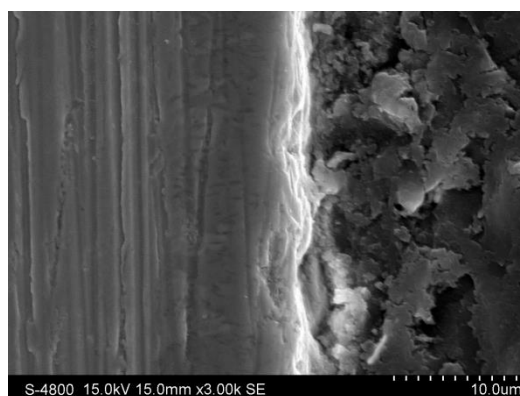


Figure 2. side-view SEM images and EDS map scanning results of the ZnAl-NO₃-LDHs film



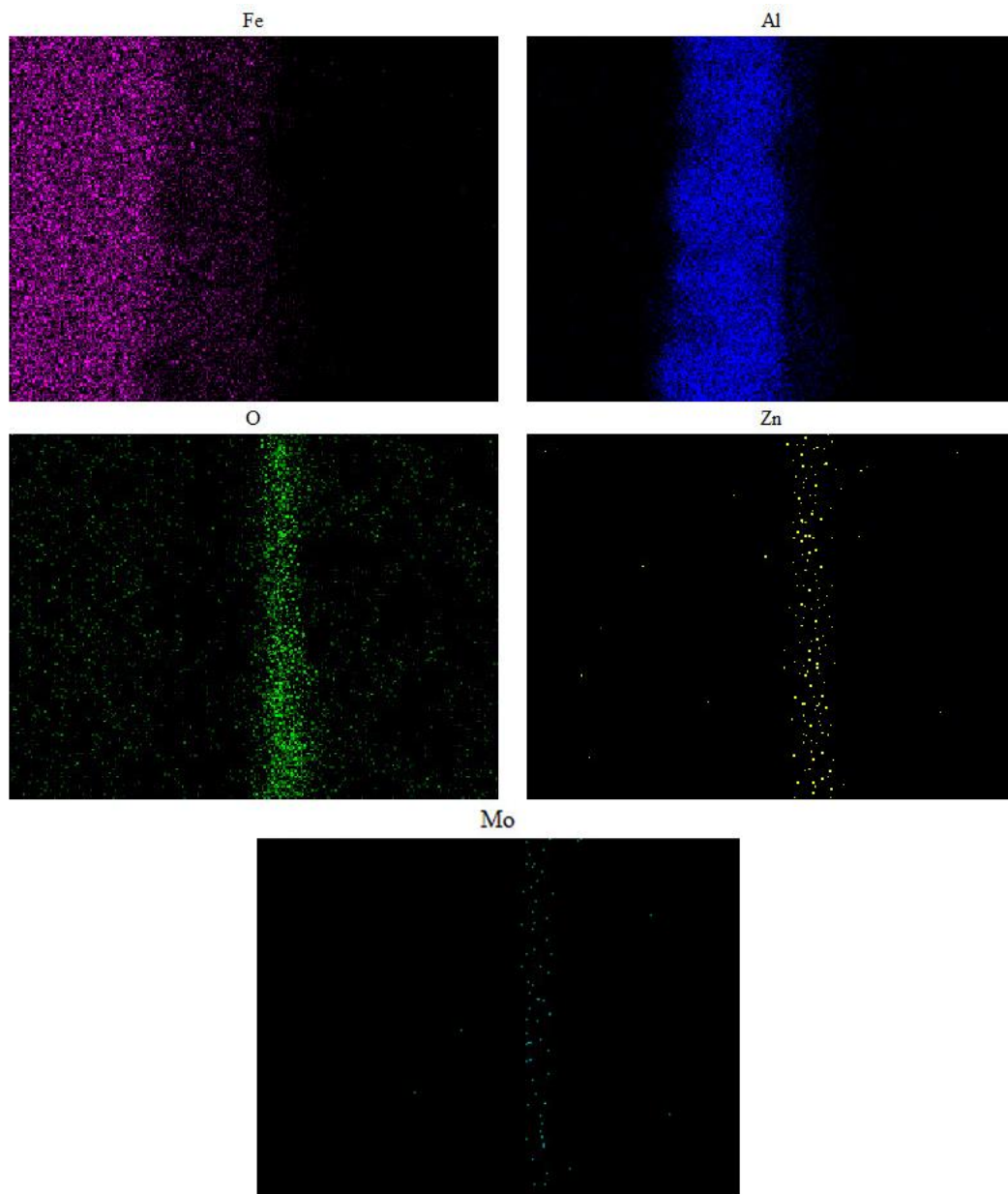


Figure 3. side-view SEM images and map scanning EDS results of the ZnAl-MoO₄-LDHs film

3.2. Phase analysis

Figure 4 presents the XRD patterns of ZnAl-NO₃-LDHs and ZnAl-MoO₄-LDHs films. In these patterns, the sharp peaks between 30° and 50° correspond to the typical reflection peaks from the iron aluminide intermetallic coating of Fe₂Al₅. The reflection peaks of Fe₂Al₅ can also be found in these films. The two strong reflection peaks at about 11° and 22° represent the typical layer structure of LDHs and are attributed to the (003) and (006) planes of the LDHs phase [26]. These findings prove that the LDHs film has successfully grown on the substrate. A comparison of the XRD patterns of these two LDHs films reveals that the diffraction peak of (003) shifts from 11.83° to 10.02°, thereby suggesting that the layer spacing of the LDHs has increased from 0.748 nm to 0.883 nm. Yan et al. synthesized ZnAl-NO₃ LDHs and ZnAl-MoO₄ LDHs powders with a layer spacing of 0.756 nm and 0.891 nm,

which are almost similar to our findings [28]. Therefore, the layer spacing can prove the exchange of intercalated anions between MoO_4^{2-} and NO_3^- .

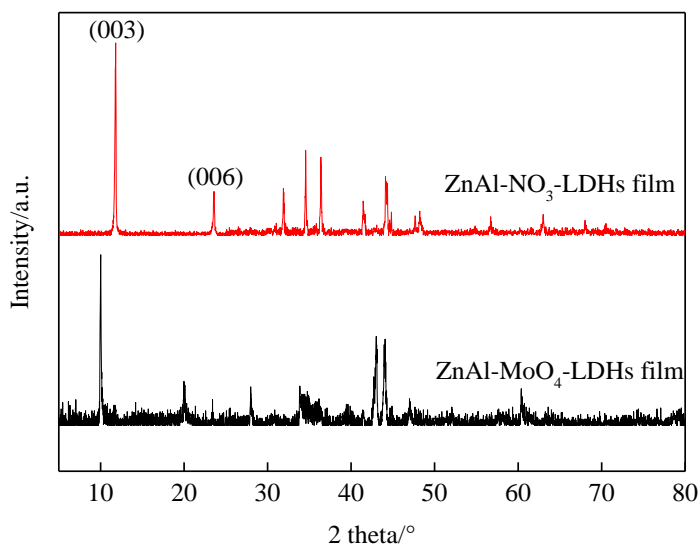


Figure 4. XRD patterns of ZnAl- NO_3 -LDHs film and ZnAl- MoO_4 -LDHs film

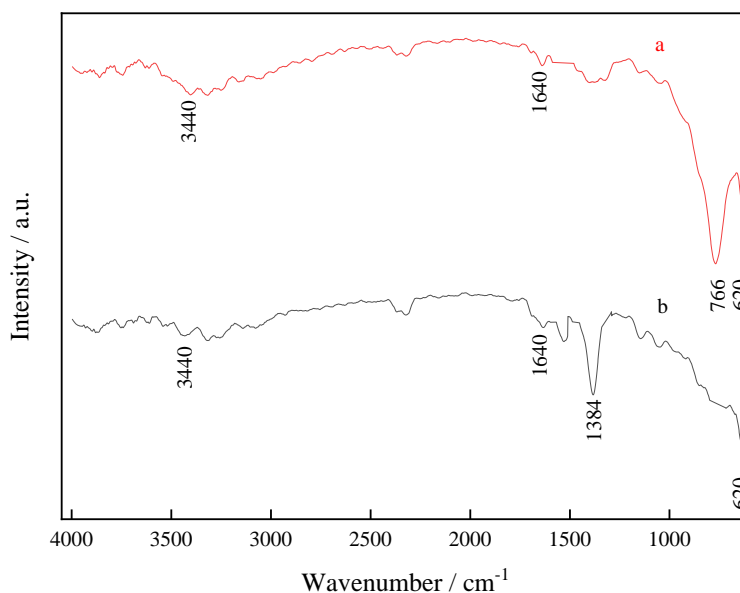


Figure 5. FT-IR spectra of (a) Aluminized Q235 steel with ZnAl- NO_3 -LDHs film; (c) Aluminized Q235 steel with ZnAl- MoO_4 -LDHs film

The FT-IR spectra of the ZnAl- NO_3 -LDHs and ZnAl- MoO_4 -LDHs films are shown in Figure 5. In both spectra, the broad absorption band at 3440 cm^{-1} can be attributed to the stretching vibration of hydroxyl groups and interlayer water molecules [23]. Meanwhile, the absorption peak at 1640 cm^{-1} can be ascribed to the bending vibration of the interlayer water, and the peak at 620 cm^{-1} can be ascribed to the typical layer lattice vibrations of M-OH in LDHs [23]. In the spectrum of the ZnAl- NO_3 -LDHs film, the absorption band at 1384 cm^{-1} can be ascribed to the stretching vibration of NO_3^- [27]. By

contrast, in the spectra of the ZnAl–MoO₄–LDHs film, the sharp absorption peak of NO₃[−] disappears, and the absorption peak observed at 766 cm^{−1} can be ascribed to the stretching vibration of MoO₄^{2−}, thereby suggesting that MoO₄^{2−} has replaced NO₃[−] as the interlayer anion in LDHs after the surface treatment process [28].

3.3. Polarization curve

Figure 6 compares the polarization curves of different samples after a 30-min immersion in a 3.5wt % NaCl solution. The comparison of three curves with that of bare Q235 steel reveals an obvious passivation area in the anodic polarization curve, thereby suggesting that a passive film has formed on the substrate. Moreover, the width of the passivation area gradually increases in the curves of the aluminized Q235 steel, the Q235 steel with ZnAl–NO₃–LDHs film, and the Q235 steel with ZnAl–MoO₄–LDHs film, thereby indicating the increasing stability of the passive film in these three samples.

The corrosion potential (E_{corr}), current density (I_{corr}), and protection efficiency (η_1) of the samples are analyzed and shown in Table 1. The Q235 steel has a corrosion potential of -0.703V—which is the most negative corrosion potential among all samples—and a high corrosion current density of 8.824 $\mu\text{A cm}^{-2}$. After the aluminizing process, the corrosion potential and corrosion current density of the Q235 steel decrease to -0.653 V and 7.189 $\mu\text{A cm}^{-2}$, respectively. Along with the growth of the ZnAl–NO₃–LDHs film, the corrosion potential of the sample increases to -0.442V, whereas its corrosion current density obviously decreases to 0.680 $\mu\text{A cm}^{-2}$. After surface treatment with Na₂MoO₄, the corrosion resistance of the sample is further improved. The sample with the ZnAl–MoO₄–LDHs film has a corrosion potential and corrosion current density of -0.416V and 0.388 $\mu\text{A/cm}^{-2}$, respectively. Yan[28] added the ZnAl–MoO₄ LDHs powder in a 3.5wt% NaCl solution as corrosion inhibitor and the corrosion current density of Q235 steel in this solution was 5.984 $\mu\text{A/cm}^{-2}$. Therefore, the ZnAl–MoO₄–LDHs film can provide better corrosion resistance for Q235 steel than the LDHs powder.

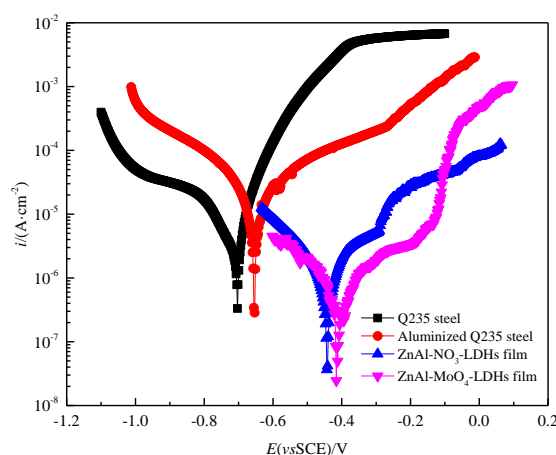


Figure 6. Polarization curves of Q235 steel, Aluminized Q235 steel, Q235 steel with ZnAl–NO₃–LDHs film and Q235 steel with ZnAl–MoO₄–LDHs film

The protection efficiencies of the aluminized Q235 steel and Q235 steel with different LDHs films to the bare Q235 steel in a 3.5wt% NaCl solution are presented in Table 1. The protection efficiencies of the aluminized Q235 steel, the Q235 steel with ZnAl-NO₃-LDHs film, and the Q235 steel with ZnAl-MoO₄-LDHs film are 18.5%, 92.3%, and 95.6%, respectively. These results prove that the LDHs film, especially the ZnAl-MoO₄-LDHs film, can effectively improve the corrosion resistance of the Q235 steel.

Table 1. the corrosion potential, current density and protection efficiency of different samples.

Sample	$E_{\text{corr}}/\text{V}_{\text{SCE}}$	$I_{\text{corr}}/\mu\text{A}\cdot\text{cm}^{-2}$	$\eta_1/\%$
Q235 steel	-0.703	8.824	
Aluminized Q235 steel	-0.653	7.189	18.5
Q235 steel with ZnAl-NO ₃ -LDHs film	-0.442	0.680	92.3
Q235 steel with ZnAl-MoO ₄ -LDHs film	-0.416	0.388	95.6

3.4. EIS spectrum

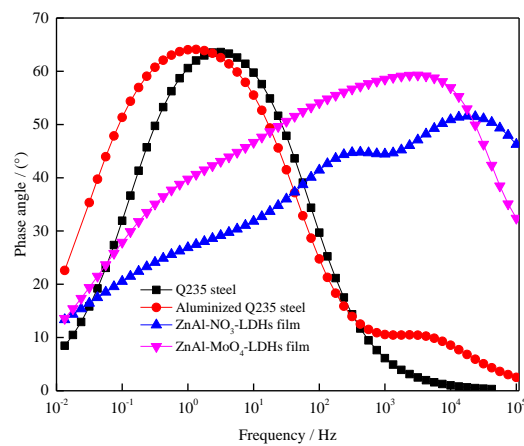
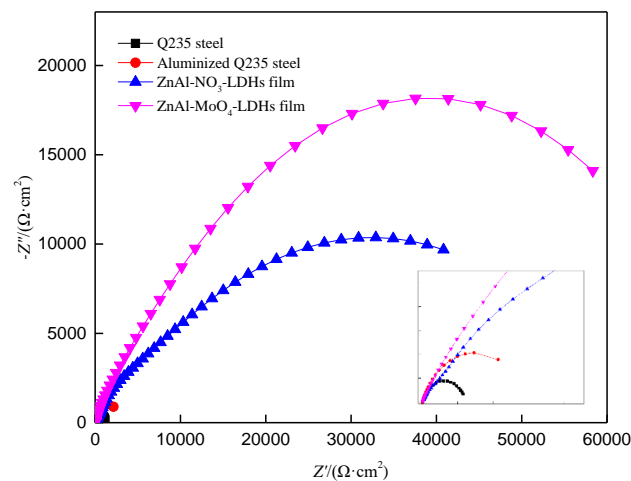
The EIS spectra of the Q235 steel, aluminized Q235 steel, Q235 steel with ZnAl-NO₃-LDHs film, and Q235 steel with ZnAl-MoO₄-LDHs film after a 1 h immersion in 3.5wt% NaCl are shown in Fig. 7. The capacitive impedance arc of the Q235 steel has the minimum radius. After the aluminizing process, the second capacitive impedance arc with a larger arc radius has appeared in the curve of the aluminized Q235 steel. After the growth of ZnAl-NO₃-LDHs and ZnAl-MoO₄-LDHs films, the EIS spectra of the samples show three capacitive impedance arcs, and the arc radius of the third capacitive impedance arc has further increased. The capacitive impedance arc at the low-frequency area has gradually increased from the bare Q235 steel to the Q235 steel with ZnAl-MoO₄-LDHs film.

Fig. 8 presents the equivalent circuits of the samples shown in Fig. 7, while Table 2 presents the electrochemical parameters that are obtained by fitting the EIS data based on these circuits. In the equivalent circuits, R_s represents the solution resistance, R_{ct} denotes the charge transfer resistance of the Q235 steel, and CPE_{dl} denotes the capacitive double layer of the Q235 steel. In the equivalent circuit of the aluminized Q235 steel, the EIS data are fitted with two time constants. The second time constant represents the aluminized layer, with R_{Al} and CPE_{Al} denoting the capacitive and resistance of the aluminized layer on the Q235 steel substrate. In the equivalent circuits of the Q235 steel with the LDHs film, the third time constant is related to the LDHs film with the capacitive CPE_{LDHs} and resistance R_{LDHs} . R_p denotes the polarization resistance, which in turn reflects the corrosion rate.

As shown in Table 2, the total resistance of the Q235 steel in the 3.5wt% NaCl solution is $1.23 \times 10^3 \Omega \text{ cm}^2$. After the aluminizing process, the polarization resistance of the aluminized Q235 steel has increased to $2.37 \times 10^3 \Omega \text{ cm}^2$. This polarization resistance increases further to $6.33 \times 10^4 \Omega \text{ cm}^2$ and $7.66 \times 10^4 \Omega \text{ cm}^2$ along with the growth of the ZnAl-NO₃-LDHs and ZnAl-MoO₄-LDHs films, respectively. Yan[28] suggested that ZnAl-MoO₄ LDHs powder can play as corrosion inhibitor in a

3.5wt% NaCl solution and the polarization resistance of Q235 steel in this solution was $1.74 \times 10^3 \Omega \text{ cm}^2$, which is much lower than that of the Q235 steel with ZnAl–MoO₄–LDHs films.

With an increasing polarization resistance, the protection efficiencies of the aluminized Q235 steel, Q235 steel with ZnAl–NO₃–LDHs film, and Q235 steel with ZnAl–MoO₄–LDHs film to the bare Q235 steel in a 3.5wt% NaCl solution have also increased. The protection efficiency of the aluminized Q235 steel is 48.1%, while those of the Q235 steel with ZnAl–NO₃–LDHs and ZnAl–MoO₄–LDHs films have increased to 98.1% and 98.4%, respectively. Therefore, similar to the findings from the polarization curve, the ZnAl–MoO₄–LDHs film provides the most effective corrosion resistance for the Q235 substrate.



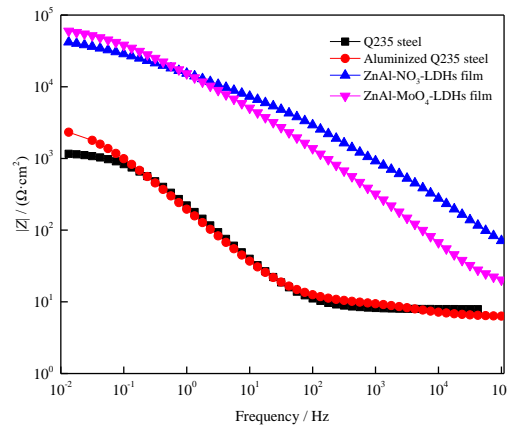


Figure 7. EIS spectra of Q235 steel, Aluminized Q235 steel, Q235 steel with ZnAl-NO₃-LDHs film and Q235 steel with ZnAl-MoO₄-LDHs film in 3.5wt% NaCl solution

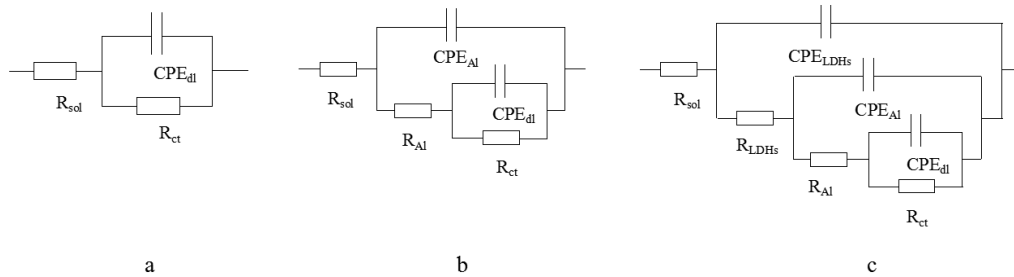


Figure 8. Equivalent circuits of Q235 steel, Aluminized Q235 steel, Q235 steel with ZnAl-NO₃-LDHs film and Q235 steel with ZnAl-MoO₄-LDHs film

Table 2. The electrochemical parameters and protection efficiency of EIS spectra.

Sample	Q235 steel	Aluminized Q235 steel	ZnAl-NO ₃ -LDHs film	ZnAl-MoO ₄ -LDHs film
$R_s/(\Omega \cdot \text{cm}^2)$	7.88	6.18	19.13	13.9
$CPE_{LDHs}/(\Omega^{-1} \cdot \text{cm}^{-2} \cdot \text{s}^n)$	Y_{LDHs}		1.83×10^{-6}	1.18×10^{-5}
$R_{LDHs}/(\Omega \cdot \text{cm}^2)$	n_{LDHs}		0.68	0.62
$CPE_{Al}/(\Omega^{-1} \cdot \text{cm}^{-2} \cdot \text{s}^n)$	Y_{Al}	1.91×10^{-5}	4.18×10^{-6}	7.33×10^{-6}
$R_{Al}/(\Omega \cdot \text{cm}^2)$	n_{Al}	0.73	0.91	0.78
$CPE_{dl}/(\Omega^{-1} \cdot \text{cm}^{-2} \cdot \text{s}^n)$	Y_{dl}	9.84×10^{-5}	2.95×10^{-5}	1.57×10^{-5}
$R_{ct}/(\Omega \cdot \text{cm}^2)$	n_{dl}	0.80	0.41	0.55
$R_p/(\Omega \cdot \text{cm}^2)$		1.23×10^3	2.36×10^3	5.89×10^4
$\eta_2/\%$		1.23×10^3	2.37×10^3	6.33×10^4
		48.10%	98.1	98.4

3.5. Immersed test

Figure 8 presents the surface morphologies of the Q235 steel, aluminized Q235 steel, Q235 steel with ZnAl-NO₃-LDHs film, and Q235 steel with ZnAl-MoO₄-LDHs film after a 7-day immersion in a 3.5wt% NaCl solution. The SEM images reveal that the surface of the bare Q235 steel is badly corroded with many corrosion pits and products on its surface. The aluminized Q235 steel shows a better corrosion resistance than the bare Q235 steel without showing obvious corrosion pits on its surface. However, a serious intergranular corrosion can be clearly observed from the SEM images along with the corrosion products. Unlike these two samples, the Q235 steel with ZnAl-NO₃-LDHs film and the Q235 steel with ZnAl-MoO₄-LDHs film show great corrosion resistance. In the SEM images, no corrosion pits or products can be found on the surfaces of these two samples and a plate-like LDHs structure can be clearly observed, thereby suggesting that the LDHs film can provide the substrate with the best corrosion resistance.

The results of the immersion test prove that the ZnAl-NO₃-LDHs and ZnAl-MoO₄-LDHs films are not corroded in 3.5wt% NaCl solution and can well protect the substrate against the corrosive solution.

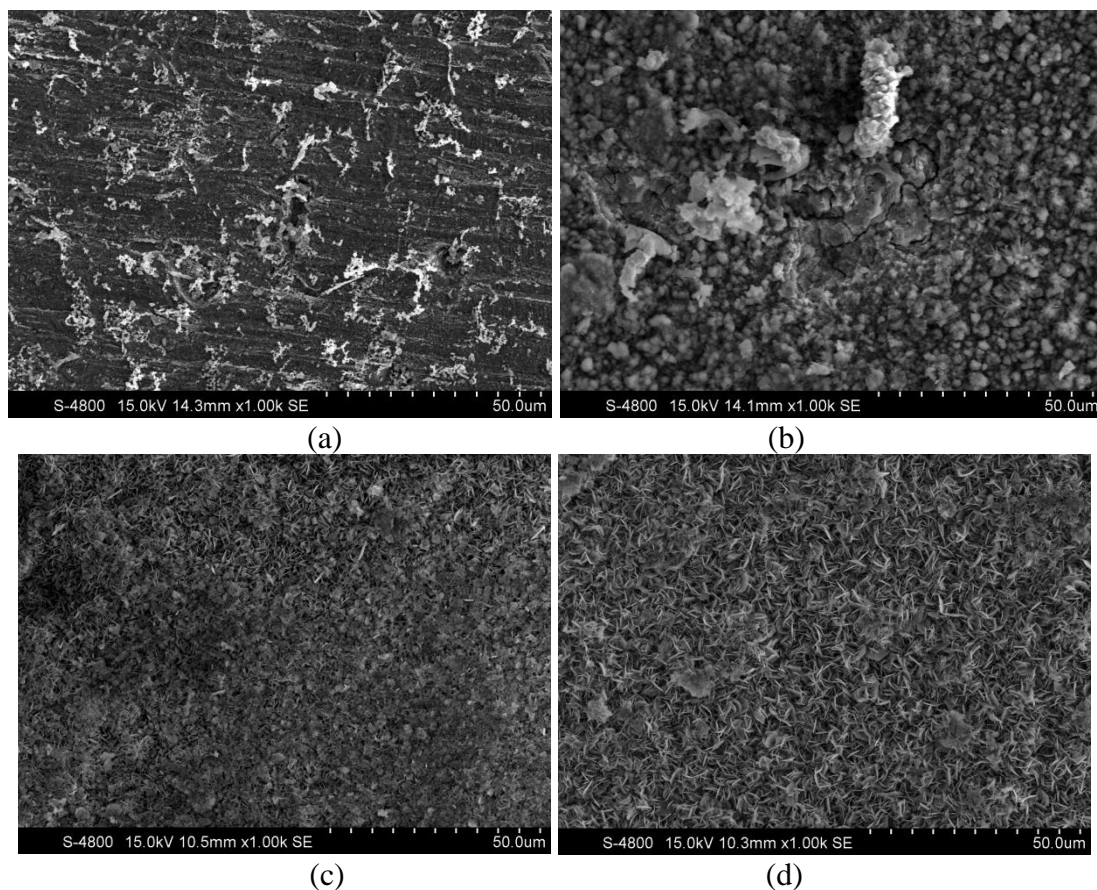


Figure 8. Surface morphology of (a) bare Q235 steel; (b) Aluminized Q235 steel; (c) Q235 steel with ZnAl-NO₃-LDHs film; (d) Q235 steel with ZnAl-MoO₄-LDHs film

3.6. Release curve

A release test of the LDHs film is performed in a 50 mL 3.5wt% NaCl solution by using a sample of the Q235 steel with ZnAl–MoO₄–LDHs film, which has an area of 10 mm×10 mm. Figure 9 shows the release curve of this film. MoO₄²⁻ demonstrates a fast release speed in the first three hours before gradually slowing down. The release process is completed in approximately 7 hours, and the final concentration of Mo is 1.4 mg/L. Therefore, the concentration of MoO₄²⁻ in the solution is 2.33 mg/L.

The loading amount of MoO₄²⁻ in the ZnAl–MoO₄–LDHs film can be calculated as

$$A = \frac{C \times V}{S}$$

where C is the concentration of MoO₄²⁻ in the solution after the immersion test, V is the volume of the test solution, and S is the area of the sample that is immersed in the test solution.

In the immersion test, the loading amount of the ZnAl–MoO₄–LDHs film is set to 0.1167 mg cm².

The release test can prove the intercalation of MoO₄²⁻ in the LDHs film and the ion exchange between MoO₄²⁻ and Cl⁻. The ion exchange can catch the corrosive Cl⁻ anion and release the MoO₄²⁻ anion into the solution, which acts as the corrosion inhibitor in the medium. MoO₄²⁻ can also help form the passive film where the LDHs film has defects and prevent the substrate from eroding further.

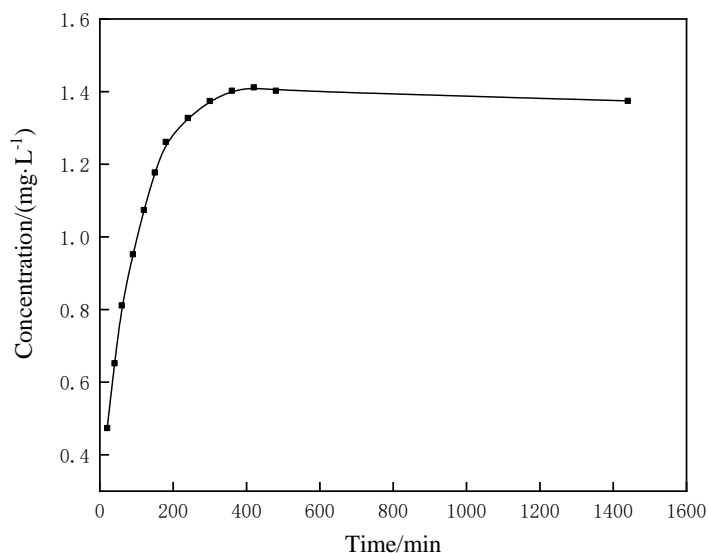


Figure 9. Release curve of Mo element in the ZnAl–MoO₄–LDHs film

4. DISCUSSION

Fig. 10 shows the growth mechanism of the ZnAl–NO₃–LDHs film. The fabrication of the LDHs film can be divided into two steps. First, the Al in the aluminized layer is corroded in the alkaline medium and the Al³⁺ is dissociated from the substrate. These cations can combine with the hydroxyl ions in the solution and form the hydroxides of aluminum. At the same time, the Zn²⁺ in the solution combines with

the hydroxyl ions to form the hydroxides of zinc. In the hydrothermal process, the hydroxides of aluminum and zinc react by co-precipitation with the intercalation of NO_3^- . After the reaction, the LDHs film is fabricated in situ on the substrate. Wu [28] suggested that the fabrication of MgAl-LDHs film follows a similar mechanism, which means the dissociative Mg^{2+} from the substrate provide sources for the formation of the original LDH granules. In the surface treatment process, the interlayered NO_3^- exchanges with the MoO_4^{2-} in the solution along with the excitation of temperature.

The in situ growth of the ZnAl-MoO₄-LDHs film can bring great corrosion resistance to the substrate. The corrosion-resistant mechanism of the ZnAl-MoO₄-LDHs film comprises two main parts as shown in Fig 11. First, the LDHs film can insulate the substrate from the corrosive medium, and the exchange between MoO_4^{2-} and Cl^- can prevent contact between the corrosive anions and the substrate. Second, Cl^- is captured into the interlayer of the LDHs film, and then MoO_4^{2-} is released into the solution. Zhou [29] proposed that MoO_4^{2-} can help form a passive film comprising $\text{Fe}_2(\text{MoO}_4)_3$ on the surface of the low carbon steel, which means that MoO_4^{2-} can form an inhibition film in the defects of the LDHs film to prevent the substrate from corroding further. Therefore, the ZnAl-MoO₄-LDHs film shows the best corrosion resistance among the examined samples.

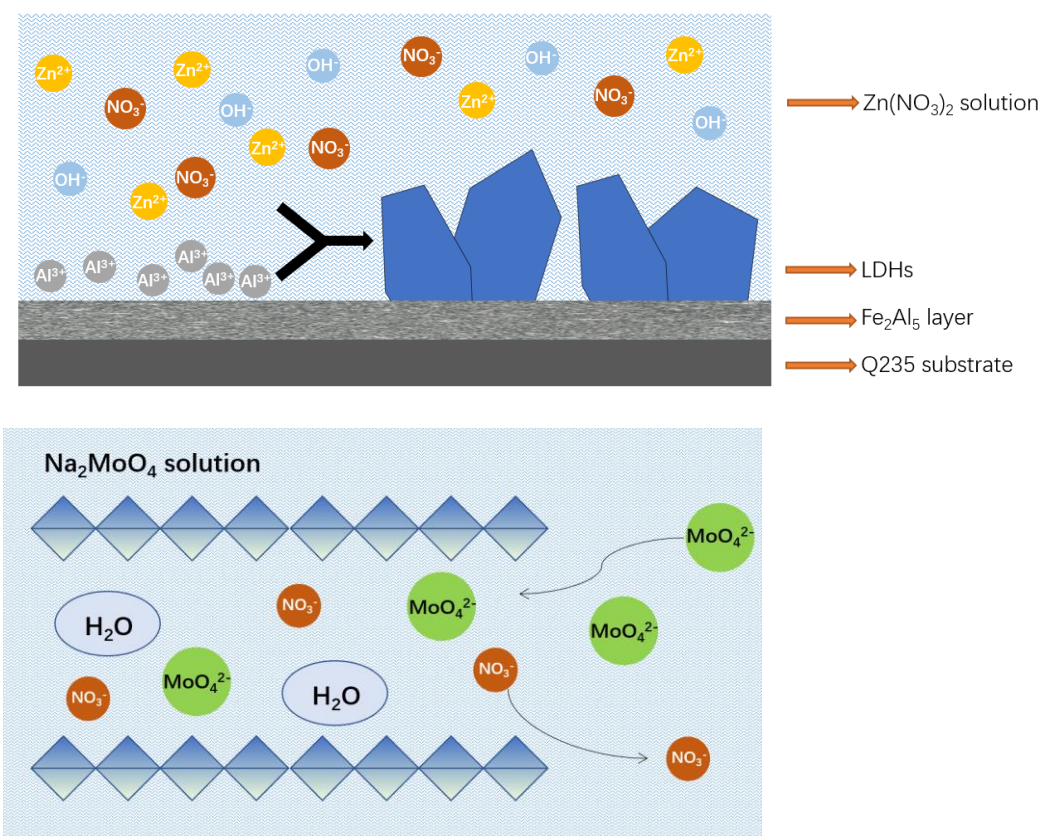


Figure 10. Growth mechanism of LDHs film

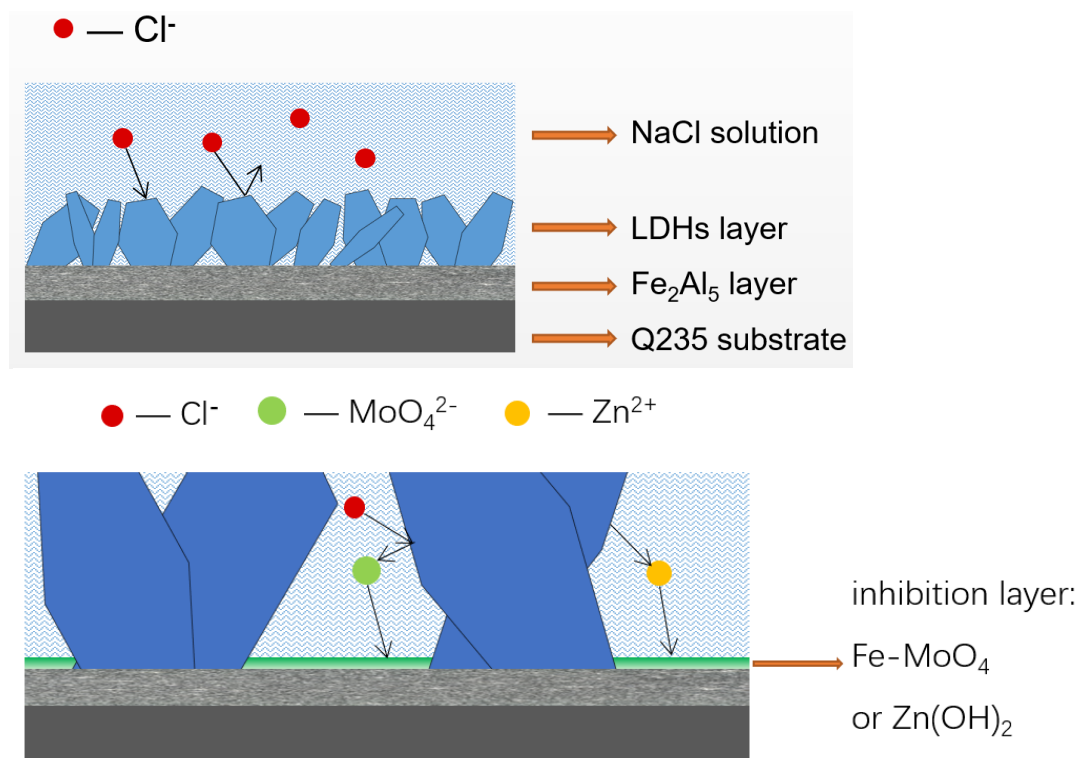


Figure 11. Anticorrosion mechanism of the ZnAl-MoO₄-LDHs film

5. CONCLUSION

1. The ZnAl-MoO₄-LDHs film is successfully fabricated in situ on the Q235 steel substrate by applying pack cementation, hydrothermal method, coprecipitation method, and ion exchange method. This film has a plate-like compact structure with a particle size of 2 μm–4 μm and average thickness of 0.1 μm.

2. Compared with the bare Q235 steel, after the growth of the ZnAl-MoO₄-LDHs film, the sample shows great corrosion resistance as the polarization resistance increases to $7.66 \times 10^4 \Omega \text{ cm}^2$. The sample achieves protection efficiencies of 98.1% and 98.4% as can be seen in the polarization curve and EIS data, respectively.

3. The ZnAl-MoO₄-LDHs film can successfully insulate the substrate from the corrosive medium. Meanwhile, the MoO₄²⁻ released by ion exchange can help form a passive film where the LDHs film has defects, which can prevent the substrate from corroding further.

ACKNOWLEDGEMENT

This work was supported by National Natural Science Foundation of China (No. 51771133 and No. 51471117) and National Basic Research Program of China (2014CB046801).

References

1. K. K. Ding, W. M. Guo, R. Qiu, J. Hou, L. Fan, L. K. Xu, *J. Mater. Eng. Perform.*, 27 (2018) 4489.

2. M. R. Dayyari, A. Amadeh and S. Sadreddini, *J. Alloys Compd.*, 647 (2015) 956.
3. L. B. Boinovich, S. V. Gnedenkov, D. A. Alpysbaeva, V. S. Egorkin, A. M. Emelyanenko, S. L. Sinebryukhov, *Corros. Sci.*, 55 (2012) 0.
4. H. B. Wang, Y. Li, G. X. Cheng, W. Wu, Y. H. Zhang, *J. Mater. Eng. Perform.*, 27 (2018) 2492.
5. S. Hao, H. Wang, L. Zhao, *Nucl. Instrum. Methods Phys. Res., Sect. B*, 368 (2016) 81.
6. B. Wang, W. B. Xue, Z. L. Wu, X. Y. Jin, J. Wu, J. C. Du, *Mater. Chem. Phys.*, 168 (2015) 10.
7. N. Wollschläger, M. Nofz, I. Dörfel, W. Schulz, R. Sojref, A. Kranzmann, *Mater. Corros.*, 69 (2018) 492.
8. E. E. Oguzie, Y. Li and F. H. Wang, *Electrochim. Acta*, 52 (2007) 6988.
9. M. Motamedi and M. M. Attar, *RSC Adv.*, 6 (2016) 44732.
10. W. Yang, Q. Li, W. Liu, J. Liang, Z. Peng, B. Liu, *Vacuum*, 144 (2017) 207.
11. Y. Liu, T. W. Yu, R. Cai, Y. S. Li, W. S. Yang, J. G. Caro, *RSC Adv.*, 5 (2015) 29552.
12. X. M. Xie, *J. Inorg. Mater.*, 14 (1999) 245.
13. E. Lima, H. Pfeiffer and J. Flores, *Appl. Clay Sci.*, 88-89 (2014) 26.
14. Y. H. Cao, S. G. Dong, D. J. Zheng, J. J. Wang, X. J. Zhang, R. G. Du, G. L. Song, C. J. Lin, *Corros. Sci.*, 126 (2017) 166.
15. L. Wang, Q. Zong, W. Sun, Z. Yang, G. Liu, *Corros. Sci.*, 93 (2015) 256.
16. Y. Cao, D. Zheng, X. Li, J. Lin, C. Wang, S. Dong, C. Lin, *Acs Appl. Mater. Inter.*, 10 (2018) 15150.
17. V. Shkirskiy, P. Keil, H. Hintze-Bruening, F. Leroux, P. Vialat, G. Lefevre, K. Ogle, P. Volovitch, *Acs Appl. Mater. Inter.*, 7 (2015) 25180.
18. X. Ye, Z. Lin, H. Zhang, H. Zhu, Z. Liu, M. Zhong, *Carbon*, 94 (2015) 326.
19. A. Lutz, O. van den Berg, J. Van Damme, K. Verheyen, E. Bauters, I. De Graeve, H. Terryn, *Acs Appl. Mater. Inter.*, 7 (2014) 175.
20. S. P. V. Mahajanam and R. G. Buchheit, *Corrosion*, 64 (2012) 230.
21. Y. Li, S. Li, Y. Zhang, M. Yu, J. Liu, *J. Alloys Compd.*, 630 (2015) 29.
22. J. Tedim, M. L. Zheludkevich, A. C. Bastos, A. D. Lisenkov, M. G. S. Ferreira, A. N. Salak, *Electrochim. Acta*, 117 (2014) 164.
23. Y. Wang and D. Zhang, *Mater. Res. Bull.*, 46 (2011) 1963.
24. X. Guo, S. Xu, L. Zhao, W. Lu, F. Zhang, D. G. Evans, X. Duan, *Langmuir*, 25 (2009) 9894.
25. L. Wu, Z. Zheng, F. Pan, A. Tang, G. Zhang, L. Liu, *Int. J. Electrochem. Sci.*, 12(2017) 6352.
26. M. L. Zheludkevich, S. K. Poznyak, L. M. Rodrigues, D. Raps, T. Hack, L. F. Dick, M. G. S. Ferreira, *Corros. Sci.*, 52 (2010) 602.
27. J. Liu, Y. Zhang, M. Yu, S. Li, B. Xue, X. Yin, *Prog. ORG. Coat.*, 81 (2015) 93.
28. H. Yan, J. Wang, Y. Zhang and W. Hu, *J. Alloys Compd.*, 678 (2016) 171.
29. Y. Zhou and Y. Zuo, *Appl. Surf. Sci.*, 353 (2015) 924.